

Propagation of a shear-horizontal surface acoustic mode in a periodically grooved AlN/Al₂O₃ microstructure

J. Xu, J. S. Thakur,^{a)} F. Zhong, H. Ying, and G. W. Auner

Department of Electrical and Computer Engineering, Wayne State University, Detroit, Michigan 48202

(Received 11 February 2004; accepted 1 April 2004)

We investigate the shear-horizontal surface acoustic waves (SH-SAWs) generated on an AlN/Al₂O₃ microstructure by laser-micromachined grooves on the AlN film. In the absence of grooves, the AlN/Al₂O₃ device shows resonance for only a lower velocity SAW mode. However, when grooves of periodicity smaller than half the wavelength of the surface acoustic wave are micromachined, a higher velocity resonance due to a SH-SAW mode is observed in the device. It is found that our SH-SAW mode remains undamped and is able to propagate across the device when loaded with a biofluidic mass. We have also measured the mass sensitivity of the SH-SAW mode under biofluidic load in terms of frequency shift. Measurements show that this mode has a very high mass sensitivity of the order 1.35 ng/ml, which suggests that the device can be applied for the detection of a small concentration of antigens in a biofluid. In this article, the fabrication and grooving techniques of the device are also addressed. © 2004 American Institute of Physics. [DOI: 10.1063/1.1753660]

I. INTRODUCTION

Investigations of the surface acoustic waves (SAWs) transducers on epitaxially grown semiconductor materials have gained widespread attention recently because of their potential applications in the field of biosensors, gigahertz range analog filters/oscillators, and acoustically induced carrier transport in low dimensional electron systems. High frequency SAWs can be generated either by employing very narrowly spaced interdigital transducers (IDTs) for a given piezoelectric material or choosing material with high SAW velocity. Minimization of the spacing between the IDTs is limited by the resolution of the fabrication techniques and becomes resource extensive below a certain limit. However, a material with higher SAWs velocity and properties such that it can be easily integrated with the substrate during fabrication process is more desirable. For such applications, a thin piezoelectric film of an AlN semiconductor is well suited due to its higher SAW velocity^{1,2} compared to other conventional piezoelectric materials like quartz and lithium niobate.³ Large band gap value of AlN semiconductor also makes it attractive for the applications of high-power and high-temperature electronic devices. In addition, AlN films are flexible in designing a piezoelectric device onto nonpiezoelectric substrates such as silicon^{4,5} and also have better mechanical properties, resistance to humidity, and high chemical stability.

In biosensing applications, the sensor sensitivity to an attached biomass of extremely small magnitude (of the order of nanograms)^{6,7} is a crucial parameter. Biosensors based on the measurements of variation in the SAWs characteristics due to the binding of biomass on the film suffer from a serious drawback because of the damping of the SAWs when the device is loaded with a biofluidic material. This damping effect arises because of coupling of surface acoustic vibra-

tions in the sagittal plane of the device with the biofluidic mass over it, which excites compressional waves in the fluid.⁸ This coupling leads to an excessive damping of the waves, which progressively increases as the waves propagate across the device and thus renders the device unsuitable for sensing of antigens or other agents in a biofluidic material. Of course, if SAW velocity is smaller than the sound velocity in the liquid then there is no coherent radiation of energy into the liquid and SAW remains undamped even when loaded with biofluid. This situation is difficult to realize, in general, as the acoustic wave velocity in solid is larger than the liquid.

Boundary conditions—a stress-free surface and a semi-infinite elastic thin film—of a simple structure of the SAW device can only support SAWs and its various other overtones, like Sezawa waves,⁹ etc., but they all suffer from the same damping problem when coupled with a fluid. However, if acoustic wave polarization is in the plane of the device surface then the only coupling that can cause damping originates from viscous effects of the fluid in contact. Thickness of the layer involved in this drag can be determined from $\xi = \sqrt{2\eta/\rho\omega}$.^{10,11} Here η and ρ are the viscosity and mass density of the fluid respectively and ω is the angular frequency of the waves. Damping due to this coupling is quite negligible and decreases with increasing value of ω due to a decrease in the amount of entrained biofluid. For this reason, it is also desired to use SAW of high frequency.

A pure shear-horizontal mode of the surface acoustic waves (SH-SAWs) does not exist on a free surface of a semi-infinite elastic solid where particle displacements are in a plane perpendicular to the sagittal plane. If boundary conditions due to the film surface are altered by introducing periodic gratings on the surface, then propagation of the shear horizontal acoustic mode across the periodic grating can be stabilized.^{12–15} On the contrary, shear mode with polarization parallel to gratings is still damped. Contrary to the Rayleigh

^{a)}Electronic mail: jagdish@wayne.edu

waves, SH-SAWs exist only for a wavelength larger than the gratings periodicity. In that case when SAW enters into the gratings (which destroy the semi-infinite elastic boundary condition created by the surface), its vertical component is absorbed by the raised mass of the gratings and SAW emerges out of the gratings with only horizontal polarization. These raised surfaces trap the Rayleigh wave's energy and transform it into the shear horizontal surface waves.

Theoretical studies¹⁶⁻¹⁸ on the surface transverse wave resonators showed that the scattering mechanism that cause damping of the surface wave not only depends on the value of the ratio of wavelength to periodicity of gratings but also sensitive to the relative values of height and periodicity of these raised surfaces. It was shown that when the height of the gratings became larger than their spacing, then higher frequency branches of dispersion curve of the shear-horizontal mode began to emerge in the frequency-wave-vector plane.^{16,17,19} However, these high frequency modes are highly damped due to their energy radiation into the substrate.¹⁹

For a thick film, shear-horizontal mode can be excited due to the relaxation of boundary conditions effects. For example, in a thin plate (thickness $h \geq 530 \mu\text{m}$) of arbitrary elastic materials, the quasishear horizontal waves are observed,²⁰ even without gratings, when the ratio of wavelength to plate thickness is less than unity.

The fabrication of the metallic gratings on the thin film surface is a problematic process and also these metallic gratings are known to produce electrical coupling with rest of the device components. Their existence also affects the amount of biomass binding on the film. However, if grooving is engraved on the film surface then there is no discontinuity in the electrical and other properties of the film. We investigated the propagation of SAW on laser micromachined grooves and its transformation into SH-SAW by varying the separation between the grooves. The basic mechanism of the conversion is similar to that of gratings, i.e., as the propagating SAW meets the groove, it gets totally damped as there is no propagation through the grooves (empty region) and the bulk waves running beneath emerge out from across the groove with only shear-horizontal polarization and thus travel across the device as SH-SAWs. This scenario is expected to hold for deep and widely separated grooves compared to the wavelength of SAW. As the SAW encounters the groove edge, part of it is scattered from the edge. But due to the roughness and other effects at the groove's edge the waves are scattered in random directions and do not form a coherent superposition to interfere with the incoming waves. In this article, we have studied the propagation of the shear-horizontal waves by fabricating grooves using laser micromachining and their frequency dispersion. We also investigate their damping behavior when loaded with fluid.

II. FABRICATION METHODS OF SAW DEVICES ON AlN/Al₂O₃ MICROSTRUCTURE

A. AlN thin film growth

AlN thin films are grown by a method of plasma source molecular beam epitaxy (PSMBE).²¹ The PSMBE system

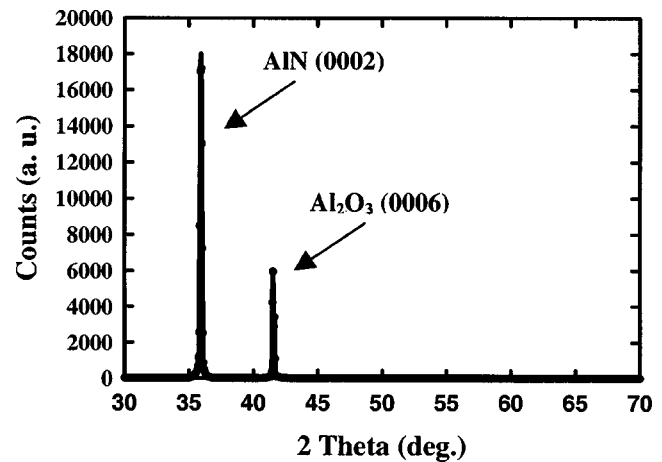


FIG. 1. X-ray diffraction data of the AlN on Al₂O₃(0001) substrate.

has a unique design of deposition source, a rod-shaped anode encircled by a hollow cathode material. By generating the argon plasma between the anode and cathode, a low energy flux of target atoms streams out of the cathode toward the substrate. The flux energy can be readily controlled by varying the substrate bias. A base ultra high vacuum at the level of 10^{-9} Torr is maintained in the PSMBE system.

Al₂O₃(0001) substrates with a surface roughness of less than 1 nm are directly loaded into PSMBE chamber and preheated at 750 °C for 1 h. N₂ and Ar gases are then delivered into the chamber at a rate of 10 sccm and 40 sccm, respectively. The generated plasma is maintained by a rf power supply with an input of 200 W at 13.5 MHz. During the growth, the substrate temperature is fixed at 650 °C and the chamber pressure is set at 1 mTorr with a throttled cryopump. These growth conditions are proved to be effective to yield high quality AlN in our PSMBE system.²² X-ray diffraction measurement in Fig. 1 gives a pronounced AlN (0002) peak with clean background free of other orientations and impurities. The peak position at 35.96° here is 0.08° smaller than the characteristic peak of the powder AlN measured. This indicates a narrow strained region at the interface of AlN and Al₂O₃.²³ The full width at half maximum of the rocking curve in Fig. 2 is 0.78°, which is comparable to other

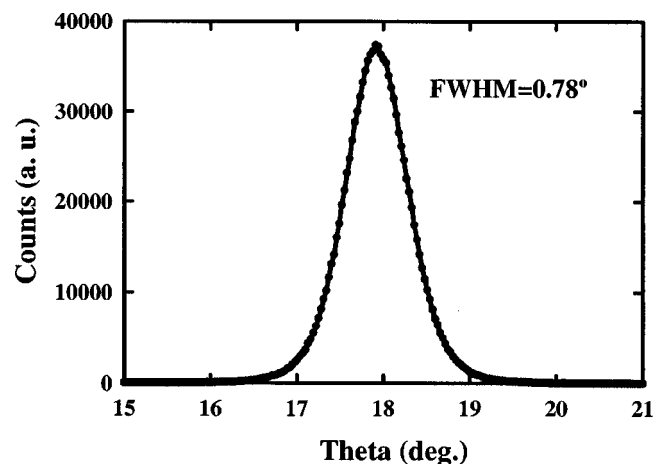


FIG. 2. Rocking curve of the AlN on Al₂O₃ (0001) structure.

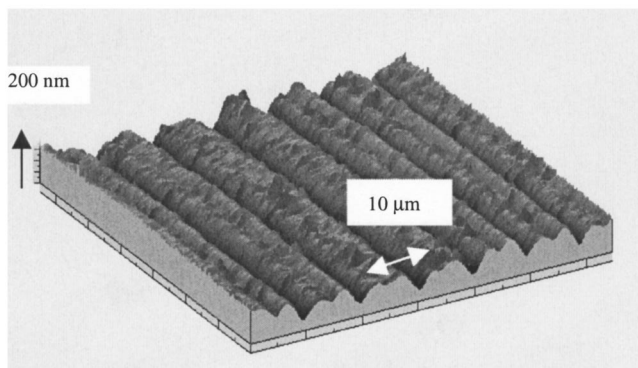


FIG. 3. AFM image of the micromachined grooves made with Eximer laser.

experimental results.²⁴ The results show that our AlN film is high quality epitaxial film with *c*-plane orientation. K. Kaya *et al.*²⁴ also found that further improvement of the crystal orientation was possible with increasing film thickness.

B. Design and fabrication of the device

Two-port delay line devices with different wavelengths have been fabricated on AlN/Al₂O₃ structure. A standard photolithography lift-off process is used to produce desired IDT patterns. Aluminum is deposited as IDT electrodes by magnetron sputtering. The thickness of Al is about 150 nm. Each device consists of two identical IDTs containing either 20 or 40 pairs of fingers. The center-to-center spacing between IDT ports is 95 λ . The acoustic aperture is 50 λ and finger width to space ratio is 1:1.

For the generation of SH-SAW, a periodic grooving structure is formed between the input IDTs and output IDTs. The structure contains 120 periodic grooves. The spatial period is 10 μm , which is 5/8 of the IDT period and the groove width to space ratio is set at 1:1. Figure 3 shows the AFM image of grooves in the depth of 150 nm micromachined by a pulse KrF excimer laser micromachining system. This system has demonstrated the capability of clean cutting with less thermal effect and precise control over customized micropattern.²⁵

III. RESULTS AND DISCUSSION

A. SAW-mode and its damping

In a SAW sensor, the operational frequency is determined by its acoustic phase velocity and lithographical resolution of the IDTs fabrication technique. It is given by a simple relation, $f = v_{\text{SAW}}/\lambda$, where the phase velocity v_{SAW} depends on the elastic properties of the film through which the wave is propagating. The level of disorder or the quality of a film can also significantly affect the value of phase velocity due to modification of the crystal symmetry and elastic constants. Figure 4 shows frequency responses of the SAW devices for varying IDTs separation without any signal processing and impedance compensation attempts for λ equal to 32, 16, and 8 μm , respectively. The ripples in the frequency passband are due to the electromagnetic feedthrough and triple transit reflections between input and output IDTs.²⁶

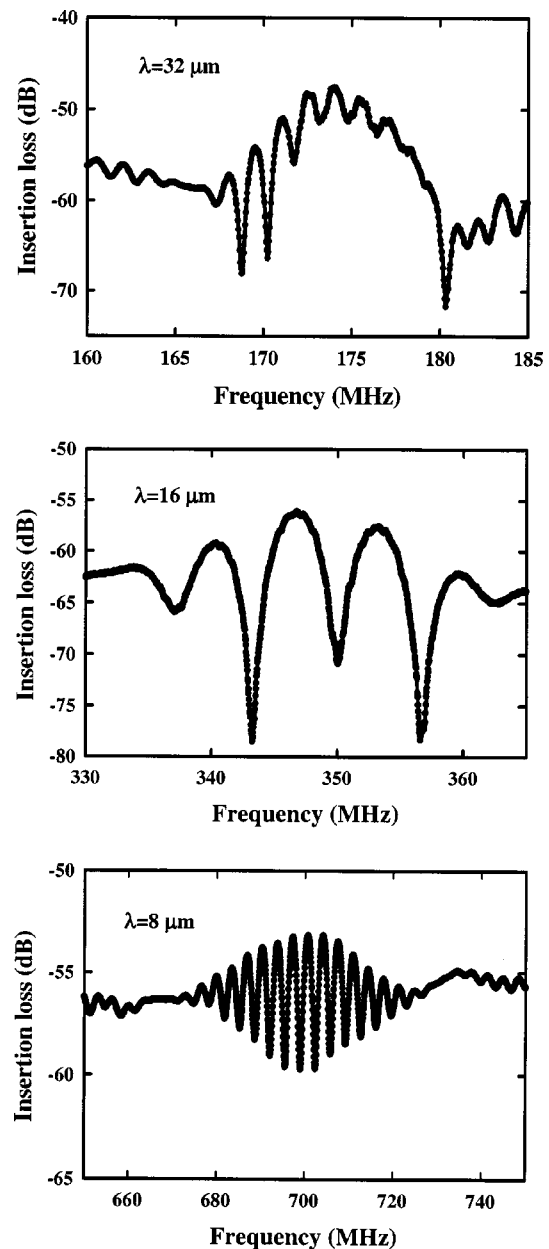


FIG. 4. Frequency response of the SAW devices for different wavelengths marked in each graph.

The characteristics of the SAW and its type can be studied from the velocity-dispersion by varying either λ or thickness h of the film. Relative variation of the SAW wavelength with respect to the film thickness not only affects the SAW phase velocity but also the effective value of the piezoelectric constant K . Over this limited range of λ variation, we studied phase velocity dispersion behavior with respect to a normalized variable kh expressed in terms of changing wave number $k = 2\pi/\lambda$ for a fixed value of $h = 1.4 \mu\text{m}$ (Fig. 5). For the determination of the phase velocity, we perform the time domain filtering to distinguish the SAW mode from the electromagnetic feedthrough and triple transit reflection. A $\sin x/x$ characteristic is clearly observed in the measured data shown in Fig. 6. The calculated phase velocities from the observed central frequencies and the corresponding wavelengths vary from 5567 to 5590 m/s. With decreasing wave-

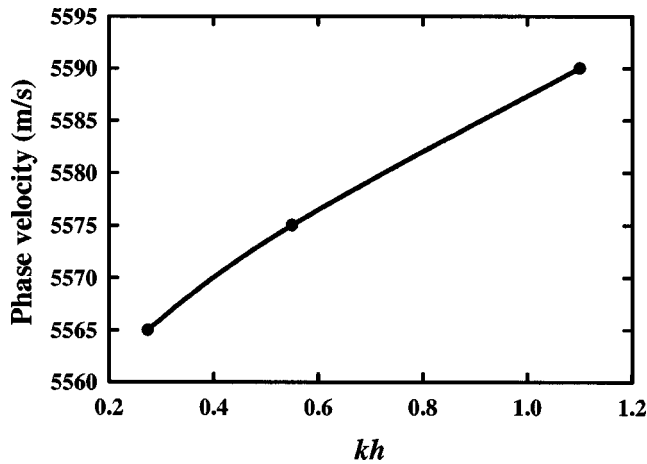


FIG. 5. Phase velocity of the SAW devices as a function of kh .

length, in a layered structure, the SAW will emerge out of the sapphire layer into the AlN film as a first-order Rayleigh mode when $\lambda \approx h$ and the value of the phase velocity will change from that of the sapphire to that of the film. Since λ variation is small in our experiments, we only observed a corresponding small increase in the SAW velocity. In our experiments, films are thinner than λ for all the samples, so the acoustic wave energy remains confined mainly to the substrate.

For a Rayleigh mode, the slow transverse bulk mode of a defects free material sets the approximate upper limit of its velocity and in the hexagonal structure of Al_2O_3 the slow transverse mode propagates along the c -axis. Its velocity 6090 m/s is much smaller than its longitudinal counterpart 11 160 m/s.^{27,28} For SAWs, the coupling between the longitudinal and the slow transverse polarizations determines its effective speed of propagation in the sagittal plane. Our much smaller measured experimental SAW velocity compared to the slow mode suggests that our SAW is dominated by transverse polarization rather than by the longitudinal component. The presence of a dominant transverse polarization in the SAW is also supported by the strong damping of these waves when loaded with fluid as discussed below. The

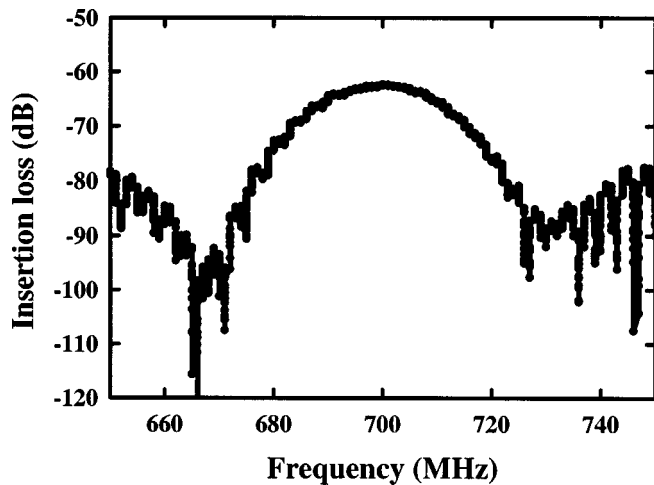


FIG. 6. Frequency response of the device after time domain filtering.

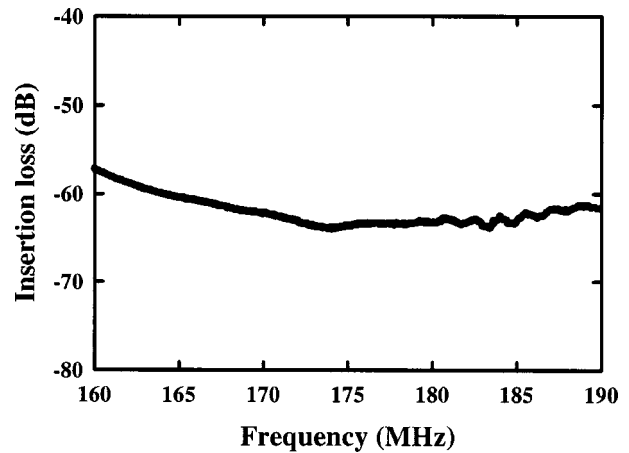


FIG. 7. Damping of the SAW-mode when loaded with fluid at $\lambda=32 \mu\text{m}$. This mode gets completely damped on loading with fluid.

acoustics velocities for the bulk AlN semiconductor are larger than the sapphire but it seems that the presence of a thin film, although with higher acoustic velocities, can significantly influence the SAW velocity.

For an anisotropic solid the SAW velocity can be estimated from $v_{\text{SAW}} = \sqrt{c_{44}f(\sigma)/\rho}$, where c_{44} is the elastic constant and $f(\sigma)$ is a function of Poisson ratio which determines the effective SAW velocity for the surface and its value lies in the range $0.76 < f(\sigma) < 0.92$.²⁸ Using elastic constant c_{44} ²⁸ and mass density ρ from Al_2O_3 , we find $f(\sigma) = 0.83$ for our experimental value of the SAW velocity. Since our samples are c -axis grown, there is no possibility of the Gulyaev–Bluestien waves,^{15,17} which exist when the c -axis of the hexagonal crystals lies in the plane of the surface.

We also investigate the damping behavior of the SAW to the fluidic load. We find that for all λ from 8 to 32 μm , SAW is totally damped by the fluid. This shows that the SAW polarization is in the sagittal plane of the device and dissipates its energy into the fluid by generating compressional waves. In Fig. 7 we show the device response when loaded with a fluid for $\lambda=32 \mu\text{m}$.

The temperature sensitivity of this SAW mode is investigated by mounting the SAW device on a thermal-electric stage and monitoring the fractional change of the operating frequency as a function of temperature at a 10 °C interval. Here f_0 is the device operating frequency at 24 °C and kh value of the SAW is 0.55. A linear relation is demonstrated in Fig. 8 and the measured temperature coefficient of frequency is $-87 \text{ PPM}/^\circ\text{C}$.

B. Generation of SH-SAW mode with grooves

In Fig. 9 we show the excitation of the higher velocity mode at $\lambda=32 \mu\text{m}$ due to the presence of grooves. The device shows two resonances—the lower frequency Rayleigh mode observed without grooves and a new higher frequency mode. The high frequency mode stabilizes at 206.500 MHz when grooves period becomes larger than half the wavelength. The calculated phase velocity of this mode is 6608 m/s, which is much higher than the first-order SAW velocity.

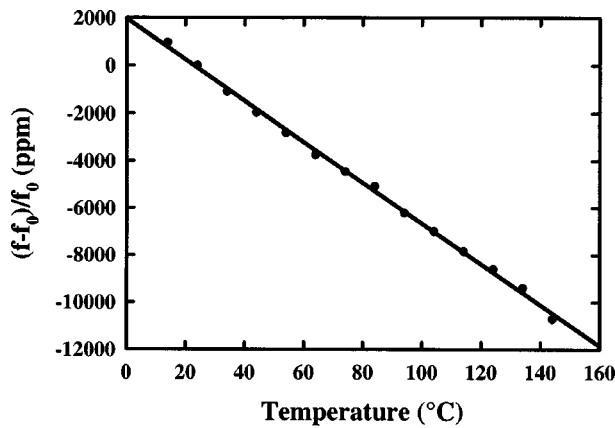


FIG. 8. Relative frequency shift behavior as a function of temperature.

Since the wavelength of the SAW is much larger than the film thickness, most of the acoustic wave energy is transported through the substrate layer. The velocity 6608 m/s of the higher frequency mode is close to the transverse bulk velocity 6466 m/s of the sapphire with polarization in the c -plane.²⁸ The fast SAW mode in our device seems to be a shear-horizontal (SH) wave with polarization in the c -plane of the sapphire whose velocity is increased by the thin film.

Our SH-SAW has features similar to the higher-order excited modes of the SAWs, which are having transverse polarizations and velocities larger than the first-order SAW velocity. However, these higher-order modes can only be excited in a layered structure where upper layer thickness is larger than the wavelength of SAW,^{29,30} a requirement not created in our device. Since the film thickness is smaller than the wavelength of the SAW, there is no possibility that our SH-SAW is a guided wave. In order to unambiguously identify this mode, accurate estimates of their (AlN and Al₂O₃) shear-velocities are required, particularly when their values are close to one another and it is the relative difference in their shear velocities that determines the type of mode and its stability. Certain amount of disorder due to AlN/Al₂O₃ interface and other effects can also affect the values of the elastic constants for the AlN film deposited on the Al₂O₃ and thus its velocities. The elastic constants for both AlN and Al₂O₃

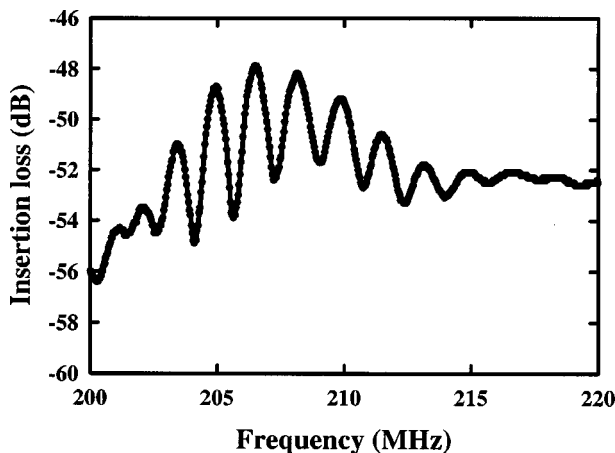
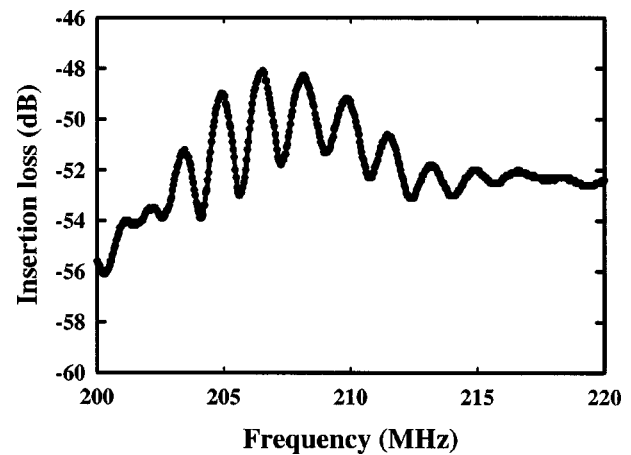
FIG. 9. Frequency response of the shear-horizontal mode for $\lambda=32 \mu\text{m}$.

FIG. 10. Damping of the shear-horizontal mode under liquid loading. This mode remained undamped under loading with fluid.

are not uniquely determined.^{27,28,31} The velocity of the shear bulk wave with polarization in the c -plane of AlN is found in the range of 6319³¹ to 6440² m/s, which is smaller than that of the sapphire -6466 ,²⁸ 6487²⁷ m/s. According to these velocities, the physical mechanism for the excitation of our SH-mode is analogous to that of the Love-wave.³² We also studied the velocity dispersion of this higher velocity mode by varying the wavelength but we found it a dispersionless mode.

We investigate the damping of the higher velocity mode by studying its propagation response to a fluidic load. In Fig. 10 we show the frequency response of the device when loaded with a fluid. The damping effect is very small as seen in the weekly damped higher velocity mode. Survival of this mode shows that it has shear-horizontal polarization in the plane of the device. In our experiments the propagation measurements are taken perpendicular to the c -axis.

C. Mass sensitivity of the SAW-modes

We investigate the mass sensitivity,³ $S = \Delta\phi/k_s\Delta\rho$, of our SAW device by depositing Al onto the central region of the device. Here ϕ and ρ are the phase delay and surface mass density of the device. Geometrical factor k_s is the fraction of the IDT spacing under mass loading, which is -0.4 in our samples. The initial phase of -83.1° corresponds to 30 nm thick Al layer on the surface to rule out the acoustoelectric³³ perturbation due to a change in surface conductivity. In Fig. 11, we show the phase shift induced after each deposition of 25 nm Al onto the inner IDT surface of area=0.016 cm². Our device shows a linear relationship between the phase shift and mass loading consistent with $\Delta\phi/\phi_0 = -\Delta v/v_0 = \Delta\rho/\rho_0$. From our measurements, we get mass sensitivity $S = 6.4^\circ/\mu\text{g}$. Given 0.1° the phase resolution of our instrument the smallest mass deposition, which can be detected is about 16 ng/cm². While the corresponding frequency sensitivity, $S = -\Delta f/k_s\Delta\rho$, based on linear phase SAW relation is about $-34 \text{ Hz cm}^2/\text{ng}$.

The typical short-term instability of oscillator circuits is within 1 Hz, that corresponds to the mass detection limit of 0.029 ng/cm², but that is an ideal situation where noise level

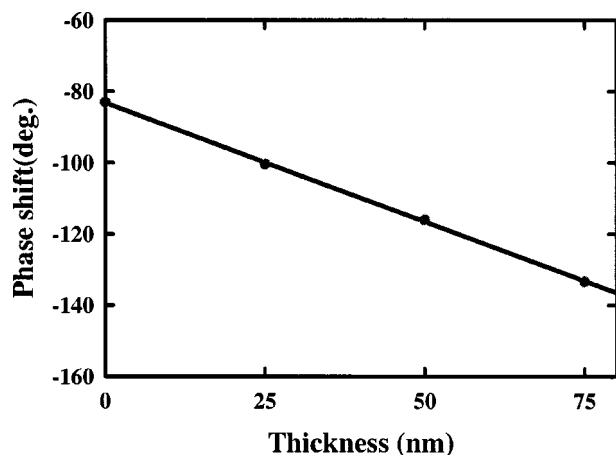


FIG. 11. Relative phase shifts as a function of sputtered Al film thickness on a 174 MHz SAW device.

is neglected. If the smallest detectable change in frequency is defined as three times the short-term instability,³⁴ then a practical limit of the resolution could become as large as 0.087 ng/cm^2 . The sensitivity values presented here are higher than reported earlier on SAW delay lines with the same wavelength on quartz substrate.^{33,35}

For application of our undamped SH-SAW mode under biofluidic load to bioagents detection, it is important to estimate the lower limit of the biomass that it can detect. We investigate the mass sensitivity of the SH-SAW mode through the frequency shift after loading $1 \mu\text{l}$ magnetic microbeads solution onto the micromachined groove region. The rigid attachment of the microbeads with the surface is ensured by placing magnetic tape underneath the device. The microbeads used herein are M-280 Sheep anti-Rabbit IgG produced by Dynal Biotech (Brown Deer, WI). The diameter, density, and solution concentration of the beads are $2.8 \mu\text{m}$, 1.3 g/cm^3 , and, 10^7 beads/ml, respectively. The measured frequency sensitivity for our SH-SAW mode turn out to be $3 \text{ Hz cm}^2/\text{ng}$, which translates to 1.35 ng/ml for beads detection. Here we take the noise level of the signal three times the instrument's resolution value. With this resolution, our device will be able to detect approximately 4500 *Escherichia coli* cells per millimeter considering the weight of each bacterium equal to 0.3 pg .³⁶

IV. CONCLUSIONS

In conclusion, we demonstrate that a higher velocity SH-SAW mode can be excited in $\text{AlN}/\text{Al}_2\text{O}_3$ layered thin film structure by micromachining parallel grooves on the AlN thin film. The acoustic polarization of this mode is in the plane of the device. In contrast to the lower velocity SAW mode which exists without grooves in the device and gets damped upon loading with fluid, this mode is able to propagate across the device without attenuation in the presence of a fluidic load and thus making the device suitable for the detection of antigens or bacteria in a biofluidic system. The mass sensitivity study also demonstrates that the device is

highly sensitive ($S = 3 \text{ Hz cm}^2/\text{ng}$), to a very small mass attachment due to the fast sound velocity in AlN and can be employed for the detection of small concentration of biological agents in a fluidic medium.

ACKNOWLEDGMENTS

This work was supported by NIH-RO1 Grant No. 1RO1EB00741-01 and the Smart Sensors and Integrated Microsystems program at Wayne State University.

- ¹ K. Tsubouchi and N. Mikoshiba, *IEEE Trans. Sonics Ultrason.* **SU-32**, 634 (1985).
- ² C. Deger, E. Born, H. Angerer, O. Ambacher, M. Stutzmann, J. Hornsteiner, E. Riha, and G. Fischerauer, *Appl. Phys. Lett.* **72**, 2400 (1998).
- ³ D. S. Ballantine, R. M. White, S. J. Marti, A. J. Ricco, E. T. Zeller, G. C. Frye, and H. Wohltjen, *Acoustic Wave Sensors: Theory, Design, and Physico-Chemical Applications* (Academic Press, San Diego, 1997).
- ⁴ L. G. Pearce, R. L. Gunshor, and R. F. Pierret, *Appl. Phys. Lett.* **39**, 878 (1981).
- ⁵ H. M. Liaw and F. S. Hickernell, *IEEE Trans. Ultrason. Ferroelectr. Freq. Control* **42**, 404 (1995).
- ⁶ G. L. Cote, R. M. Lee, and M. V. Pishko, *IEEE Sensors Journal* **3**, 251 (2003).
- ⁷ J. C. Andle and J. F. Vetelino, *Sens. Actuators, A* **44**, 167 (1994).
- ⁸ A. J. Ricco and S. J. Martin, *Appl. Phys. Lett.* **50**, 1474 (1987).
- ⁹ K. Sezawa, *Bull. Earthquake Res. Inst., Univ. Tokyo* **3**, 1 (1927).
- ¹⁰ S. J. Martin, A. J. Ricco, T. M. Niemczyk, and G. C. Frye, *Sens. Actuators* **20**, 253 (1989).
- ¹¹ G. McHale, M. Newton, and F. Martin, *J. Appl. Phys.* **93**, 675 (2003).
- ¹² B. A. Auld, J. J. Gagnepain, and M. Tan, *Electron. Lett.* **12**, 650 (1976).
- ¹³ Y. V. Gulyaev and V. P. Plesskii, [*Sov. Phys.* **23**, 266 (1978)].
- ¹⁴ A. A. Maradudin, *Surface Waves in Plasmon and Solids* (World Scientific, Singapore, 1986).
- ¹⁵ Y. V. Gulyaev, *IEEE Trans. Ultrason. Ferroelectr. Freq. Control* **45**, 935 (1998).
- ¹⁶ B. A. Auld, J. J. Gagnepain, and M. Tan, *Acoustic Fields and Waves in Solids* (Krieger, Malabar, 1990).
- ¹⁷ Y. V. Gulyaev and V. P. Plesskii, *Pis'ma Zh. Tekh. Fiz.* **3**, 220 (1977) [*Sov. Tech. Phys. Lett.* **3**, 87 (1977)].
- ¹⁸ B. A. Auld, A. Renard, and J. Henaff, *Electron. Lett.* **18**, 183 (1982).
- ¹⁹ A. R. Baghai-Wadji and A. A. Maradudin, *Appl. Phys. Lett.* **59**, 1841 (1991).
- ²⁰ B. D. Zaitsev, S. G. Joshi, and I. E. Kuznetsova, *Smart Mater. Struct.* **6**, 739 (1997).
- ²¹ P. K. Guo, G. W. Auner, and Z. L. Wu, *Thin Solid Films* **253**, 223 (1994).
- ²² M. Lukitsch, Y. Danylyuk, V. Naik, C. Huang, G. Auner, L. Raimai, and R. Naik, *Appl. Phys. Lett.* **79**, 632 (2001).
- ²³ F. S. Hickernell, *Proceedings, IEEE Ultrasonic Symposium* (IEEE, New York 1996), pp. 235–242.
- ²⁴ K. Kaya, Y. Kanno, H. Takahashi, Y. Shibata, and T. Hirai, *Jpn. J. Appl. Phys., Part 1* **35**, 2782 (1996).
- ²⁵ Q. Zhao, M. Lukitsch, J. Xu, G. Auner, R. Niak, and P. K. Kuo, *MRS Internet J. Nitride Semicond. Res.* **5**, art. no.-W11.69 (2000).
- ²⁶ C. Campbell, *Surface Acoustic Wave Devices and their Signal Processing Applications* (Academic Press, New York, 1989).
- ²⁷ J. M. Winey, Y. M. Gupta, and D. E. Hare, *J. Appl. Phys.* **90**, 3109 (2001).
- ²⁸ J. B. Wachtman, *J. Res. Natl. Bur. Stand., Sect. A* **64**, 213 (1960).
- ²⁹ G. F. Iriarte, *J. Appl. Phys.* **93**, 9604 (2003).
- ³⁰ O. Elmazria, V. Mortet, M. Hakiki, M. Nesladek, and P. Alnot, *IEEE Trans. Ultrason. Ferroelectr. Freq. Control* **50**, 710 (2003).
- ³¹ A. F. Wright, *J. Appl. Phys.* **82**, 2833 (1997).
- ³² G. McHale, M. Newton, and F. Martin, *Appl. Phys. Lett.* **79**, 3542 (2001).
- ³³ A. J. Ricco and S. J. Martin, *Thin Solid Films* **206**, 94 (1991).
- ³⁴ M. J. Vellekoop, *Ultrasonics* **36**, 7 (1998).
- ³⁵ H. Wohltjen, *Sens. Actuators* **5**, 307 (1984).
- ³⁶ F. C. Neidhardt and J. L. Ingraham, *Escherichia Coli and Salmonella: Typhimurium Cellular and Molecular Biology* (American Society for Microbiology, Washington DC, 1987).